Available online at www.sciencedirect.com
ScienceDirect
Journal of Magnetic Resonance 185 (2007) 94–102
JMR Journal of Magnetic Resonance
www.elsevier.com/locate/jmr

Nonlinear magnetic field gradients can reduce SAR in flow-driven arterial spin labeling measurements

Kenneth I. Marro *, Donghoon Lee, Outi M. Hyyti

Department of Radiology, Box 357115, University of Washington, Seattle, WA 98195-7115, USA

Received 20 July 2006; revised 22 November 2006
Available online 18 December 2006

Abstract

This work describes how custom-built gradient coils, designed to generate magnetic fields with amplitudes that vary nonlinearly with position, can be used to reduce the potential for unsafe tissue heating during flow-driven arterial spin labeling processes. A model was developed to allow detailed analysis of the adiabatic excitation process used for flow-driven arterial water stimulation with elimination of tissue signal (FAWSETS) an arterial spin labeling method developed specifically for use in skeletal muscle. The model predicted that, by adjusting the amplitude of the gradient field, the specific absorption rate could be reduced by more than a factor of 6 while still achieving effective labeling. Flow phantom measurements and in vivo measurements from exercising rat hind limb confirmed the accuracy of the model's predictions. The modeling tools were also applied to the more widely used continuous arterial spin labeling (CASL) method and predicted that specially shaped gradients could allow similar reductions in SAR.

Keywords: Arterial spin labeling; Perfusion; Custom-built gradient; Specific absorption rate; Nonlinear magnetic field; FAWSETS; CASL

1. Introduction

The purpose of this study was to determine if custom-built gradient coils, designed to generate magnetic fields that vary with position in specific, nonlinear fashions, could reduce the potential for unsafe tissue heating during flow-driven adiabatic manipulations of arterial water magnetization. RF energy is absorbed nearly continuously during flow-driven arterial spin labeling measurements and this can lead to unacceptable levels of tissue heating [1,2]. Our goal was to test whether nonlinear magnetic field gradients, generated by specially designed gradient inserts, could reduce the minimum B_1 amplitude required to achieve effective labeling. The B_1 amplitude varies linearly with current flow in the RF coil while the specific absorption rate (SAR) varies with the square of the current so even a modest reduction in B_1 amplitude could significantly reduce tissue heating, allowing safer and broader applications of arterial spin labeling (ASL) measurements.

The potential for tissue heating presents a substantial limitation for continuous arterial spin labeling (CASL) measurements and is an increasing cause for concern as higher field (3.0T and higher) magnets become more broadly available for human measurements. In order to reduce SAR it may be necessary to increase the sequence repetition time, which degrades time resolution, or to reduce the amplitude of the B_1 field used for labeling, which can reduce the labeling efficiency and degrade the signal to noise (S/N) ratio [3–5]. Use of two RF coils, one for labeling and one for signal acquisition, can also reduce SAR but this may not allow labeling in all the arteries that feed the tissue of interest and could lead to errors in the perfusion measurement due to collateral circulation [1,6,7]. SAR effects tend to be even more limiting for flow-driven arterial water stimulation with elimination of tissue signal (FAWSETS), which has been a focus of research in our laboratory [8–10].

* Corresponding author. Fax: +1 206 543 3495.
E-mail address: marro@u.washington.edu (K.I. Marro).

1090-7807/$ - see front matter © 2006 Elsevier Inc. All rights reserved.
doi:10.1016/j.jmr.2006.11.011

Both CASL and FAWSETS require a spatially variant static magnetic field, ΔB_0, superimposed over the main magnetic field, B_0, to accomplish the desired flow-driven, adiabatic labeling. In CASL labeling the ΔB_0 field is typically supplied by the magnet system's built-in linear gradients. Custom-built gradients have previously been implemented in CASL measurements [11–15] but they were deliberately designed to generate linear ΔB_0 fields. In FAWSETS labeling the ΔB_0 field arises as a consequence of the shimming process; shimming leaves a gradient in the B_0 field at the edges of the shimmed volume. While both the linear gradients used in CASL and the shim-generated ΔB_0 fields used for FAWSETS are adequate for flow-driven adiabatic spin labeling, neither field is optimized for the task.

Arterial spins flowing through a spatially variant ΔB_0 field experience time variant changes in their static magnetic field. As such, the ΔB_0 field plays the role of the frequency sweep component of adiabatic RF pulses [16–18]. The function used to modulate the frequency sweep during an RF pulse can be optimized in order to reduce the B_1 amplitude required to maintain adiabatic conditions. We have designed custom gradient configurations that allow this same basic principle to be applied to flow-driven, adiabatic manipulations.

We have previously described other advantages (not related to SAR) of a nonlinear custom gradient we designed and built for use in FAWSETS measurements of perfusion in rat hind limb [19]. In this work we have developed a model describing how changes in current flow in our gradient affect the flow-driven adiabatic labeling process. We used our model to evaluate the adiabaticity ratio, κ, as defined previously [17,18], and predicted that adjusting the amplitude of ΔB_0 by properly setting the gradient current would allow adiabatic conditions (i.e., $\kappa \ll 1$) to be maintained with lower B_1 amplitude. We tested this prediction using flow phantom measurements and in vivo measurements from exercising rat hind limb. Our results consistently show that the nonlinear ΔB_0 field produced by our gradient can be used to substantially reduce SAR during the FAWSETS labeling process.

While the primary focus of this work is on FAWSETS measurements, the basic principles are the same for CASL. We have applied our modeling methods to CASL measurements and we include those results predicting that similar reductions in SAR could be achieved for this labeling process.

2. Methods

All MR measurements were conducted on our 4.7T, horizontal bore, Bruker magnet controlled by a Varian Inova console running VNMR version 6.1. Our custom-built gradient (Fig. 1) was designed specifically for use with an RF coil built for rat hind limb measurements, which was a 2.5 cm diameter, 2.5 cm long saddle coil tuned to the water resonance (200.1 MHz). Details of the design process for the custom-built gradient have been published previously [19].

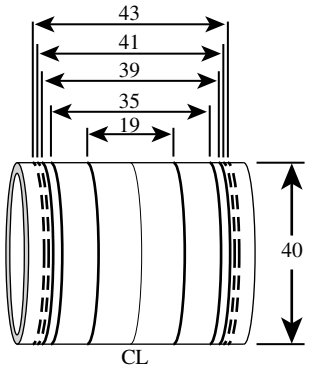

Fig. 1. This diagram shows the geometry of the gradient coil implemented in the FAWSETS flow phantom and in vivo measurements. The gradient was designed so that a 2.5 cm diameter by 2.5 cm long saddle coil, including the tune and match capacitors, could be centered inside it. The device consists of 10 conducting loops. Current in the dashed line elements flows in the opposite direction to that in the solid line elements. Spacing of the current loops is symmetric about the center-line (CL) of the gradient. Dimensions are given in mm. The device consisted of 20-gauge copper wire hand wound around a plexiglass tube. A custom-built, current-controlled power supply was used to drive the gradient. The power supply had a range of currents from −1.5 to +1.5 A.

2.1. Modeling of the gradient-enhanced FAWSETS labeling process

The first step in modeling the adiabatic labeling process was to measure the spatial variations in B_1 and ΔB_0. The shape of the B_1 field was measured by acquiring a profile from a 1 cm diameter test tube filled with water. The profile was acquired using a frequency-encoding gradient along the z-axis (the direction of flow in all the experiments) following a hard 90-degree excitation pulse. The profile was fed into an iterative fitting routine that calculated the B_1 field, taking into account spatial variations in both the transmission and reception sensitivities of the RF coil.

Measurements of ΔB_0 were obtained from the same test tube of water by acquiring a series of z-axis profiles with the delay time between excitation and acquisition incremented from 10 to 207.5 ms in 2.5 ms steps. A 2D Fourier transform of the raw data yielded frequency, with 5 Hz resolution, as a function of position. Other acquisition parameters included 40 mm field of view, TR = 4 s, SW = 60 kHz, 128 points and 8 signal averages.

The modeling, based on these measurements of B_1 and ΔB_0, assumed that there was no substantial radial variation of the fields. To assess radial variations in B_1, spin echo images were acquired from a 2 cm diameter static water phantom (data not shown). These images verified that, within the axial sweet spot as shown in Fig. 2A, the amplitude of the B_1 field remained above 95% of maximum within a 1.8 cm diameter at the center of the coil. This is larger than the diameters of the rat legs used in this study, which

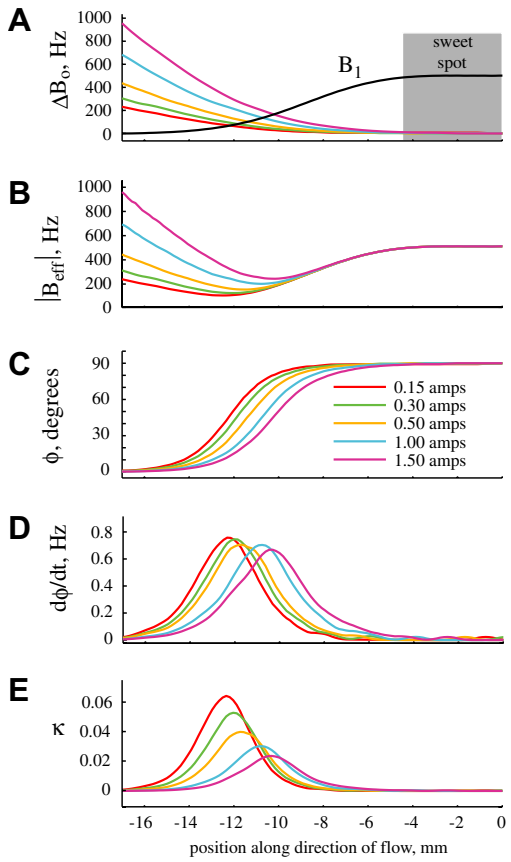

Fig. 2. (A) Shows the measured spatial variations in the ΔB_0 field with 5 different currents flowing through the custom-built gradient. The measured B_1 field generated by our RF coil is also shown in (A) along with the axial sweet spot, defined as the region where B_1 remains within 5% of maximum. Only the left-hand sides of the symmetric fields are shown and the 0 position corresponds to the center of the sweet spot of the RF coil. (B–E) show the intermediate calculations involved in the modeling and illustrate how gradient current affects the labeling process. (B) shows the spatial variations in the magnitude of B_{eff} and (C) shows ϕ, the angle that B_{eff} forms with the positive z-axis. Both B_{eff} and ϕ were calculated directly from the B_1 and ΔB_0 fields in (A). (D) shows the time rate of change of ϕ assuming a constant flow velocity of 10 cm/s from left to right. Note that as gradient current increased the magnitude of B_{eff} increased within the labeling slice and the curves for both ϕ and $d\phi/dt$ shifted to the right. The net result of these two effects is that the peak value of the adiabaticity ratio, κ in (E) decreased from about 0.6 to 0.2 over the range of gradient currents tested. The key point of these graphs is that, for a fixed B_1 field and velocity, optimizing the gradient current reduces the nominal amplitude of κ.

were approximately 1.25 cm. No attempt was made to acquire off-axis measurements of ΔB_0 but modeling results verified that, within the homogenous B_1 region, ΔB_0 varied by less than 2%. The smaller radial variation in ΔB_0, compared to B_1, is to be expected since the conducting elements for the gradient have a larger diameter (4.0 cm) than the RF coil elements (2.5 cm).

The measured spatial variations of B_1 and ΔB_0, along with an assumed velocity of flow, were used as inputs to a Matlab-based (Matlab version 6.5.0, The MathWorks, Inc.) program we previously developed to model flow-driven adiabatic manipulations of arterial water [20]. The program first calculated the effective field [17,18], B_{eff}, defined by B_1 (transverse component) and ΔB_0 (longitudinal component). Based on this definition, the model calculated the spatial variations in the magnitude of B_{eff} and the angle, ϕ, that it formed with the positive z-axis.

The program then calculated $d\phi/dt$, or the time rate of change in ϕ that arterial spins would experience as they flowed through the spatially variant magnetic fields. These calculations involved taking the derivative of ϕ with respect to position (yielding degrees/mm) and then appropriate scaling of the result to convert the units into Hz. The conversion from degrees/mm to Hz required the assumption of a reasonable velocity of flow. In all the examples presented in this work, a velocity of 10 cm/s was assumed. The final step in the modeling process was to calculate the adiabaticity ratio, κ, defined as $d\phi/dt$ divided by the magnitude of B_{eff}.

2.2. Flow phantom measurements

Flow phantom measurements were conducted to verify the modeling results under well-defined conditions. The flow phantom consisted of a 1 cm diameter tube through which water was pumped at an average velocity of 5 cm/s. The tube was centered in the combined RF/gradient probe. Laminar conditions were maintained in the phantom and the resulting parabolic flow profile meant that the maximum velocity was 2 times the average velocity or 10 cm/s. To eliminate signal attenuation due to these relatively high velocities, the pulse sequence used for these particular measurements was modified to include flow-compensated crusher gradients. Gradient-enhanced FAIRSETS perfusion measurements were acquired with the RF amplifier power incremented from −16 to 13 dB. The amplitude of B_1 at the 10 dB power setting was calculated after determining the duration of a 90-degree pulse. Straightforward calculations based on the definition of dB then showed that the range of amplifier power settings corresponded to a range of B_1 from about 6 to 175 Hz. The measurements were repeated for 5 different current amplitudes (0.15, 0.30, 0.50, 1.0 and 1.5 A) flowing through the custom-built gradient. The labeling efficiency [2,20,21] was determined by dividing the perfusion signal by the signal acquired following a hard 90-degree pulse. The 2 s long labeling period was followed by a slice selective (5 mm slice thickness) 180-degree pulse to localize the signal within the sweet spot of the RF and gradient coils. Other acquisition parameters included 40 mm field of view, TR = 4 s, TE = 15 ms, SW = 60 kHz, 128 points and 8 signal averages.

2.3. Rat hind limb measurements

Measurements of perfusion during stimulated exercise were conducted to test whether our custom ΔB_0 field could reduce the B_1 amplitude required for labeling in vivo. The procedures for all animal experiments were in accordance

with guidelines of the University of Washington Animal Care Committee and the National Institutes of Health. The general protocol was very similar to that of the flow phantom protocol described above: single-voxel, gradient-enhanced FAWSETS perfusion measurements were acquired with a range of different B_1 amplitudes (5, 10, 15, 20 and 25 dB) applied during the labeling period and with 4 different currents (0.30, 0.50, 1.0 and 1.5 A, acquired in random order) flowing through the custom-built gradient. The B_1 amplitude at 20 dB was calculated after determining the duration of a 90-degree pulse. Calculations based on the definition of dB then showed that the range of amplifier power settings corresponded to a range of B_1 from about 50 to 940 Hz.

2.3.1. Stimulation protocol

The purpose of the stimulated exercise was to increase the available signal by increasing perfusion of the hind limb. The stimulation protocol has previously been described in detail [10]. Briefly, the animals were anesthetized with isoflurane and a bipolar electrode was surgically implanted around the right sciatic nerve. The right leg was placed in the combined RF/gradient probe and centered in the magnet bore. A water balloon was placed under the right foot and attached to a pressure transducer to monitor the relative force of contraction. Stimulated contractions of all the lower leg muscles were induced by 250 ms long excitation pulse trains with pulse duration of 0.1 ms. For each animal, the maximum stimulated contraction was determined at the beginning of the experiment with the pulse frequency set to 300 Hz. Moderate force contractions were then induced at a rate of one contraction every 5 s with the pulse frequency actively adjusted to maintain constant contractile force at 20% of the maximum stimulated contraction. This stimulation protocol has previously been shown to increase rat hind limb perfusion from about 20 to 60 ml/100 g/min and that perfusion reaches a steady state after about 4 min of persistent stimulation [10].

2.3.2. Perfusion measurement protocol

Continuous, flow-driven, adiabatic excitation of the inflowing arterial water was achieved by 2.0 s of continuous, on-resonance RF with variable current flowing through the custom-built gradient. Two signals were acquired between each stimulated contraction. The direction of current flow in the custom-built gradient was alternated for each acquisition in order to modulate the phase of the perfusion component of the signal. Phase cycling, as described previously [19], was then used to eliminate all other components of the signal.

The labeling period was followed by a slice selective 180-degree pulse to localize the signal from a 5 mm thick slice located at the proximal edge of the sweet spot of the RF coil. Symmetric crusher gradients ($b = 5$ s/mm^2, 2.5 G/cm, 4 ms duration, 8.5 ms separation) around the slice-select pulse were used to attenuate signal outside the slice and to filter out signal from faster flowing arterial water [22]. Data were acquired as free induction decays (FID's) during the second half of the spin echo generated by the 180-degree pulse. Acquisition parameters included 4000 Hz sweep width, 1000 complex points, echo time (TE) = 14.0 ms and no signal averaging. Repetition time (TR) was 2.5 s and, during stimulation periods, was gated by the stimulation pulse generator so that signal excitation and acquisition were interleaved between muscle contractions.

2.3.3. SAR estimate

Power dissipation in the hind limb tissue was estimated by measuring the loaded and unloaded Q of the RF coil [23]. The unloaded Q was 194 and the Q when the coil was loaded with a rat hind limb was 76 so the fractional power dissipated in the tissue was 61%. The maximum power output from the RF amplifier was 1000 W and the nominal power setting used during the perfusion measurements with the custom-built gradient turned off was 33 dB below maximum. The maximum power dissipated in the hind limb was therefore about 1 W/kg of body weight (300 g rats) and when current was applied to the custom-built gradient power dissipation was reduced by the square of the reduction in B_1 amplitude. This estimate ignores resistive losses in the cables but gives a rough estimate of SAR during the perfusion measurements.

3. Results

Our modeling results demonstrate the basic principles involved in our analysis and predict that specially shaped magnetic field gradients can allow substantial reductions in B_1 amplitude—and hence reduce SAR—during flow-driven, adiabatic spin labeling processes. Fig. 2 predicts that, as gradient current increases (while all other parameters are held constant), the magnitude of B_{eff} will increase within the labeling slice and the curves for both ϕ and $d\phi/dt$ will shift to the right. The net result of these two effects is that the maximum amplitude of κ will decrease as the gradient current increases. These modeling results suggest that, by optimizing the gradient current, adiabatic conditions should be maintained for spins flowing at higher velocities. Or conversely, for a fixed velocity, optimizing the gradient current should allow adiabatic conditions to be met with lower B_1 amplitude, and hence lower SAR (see Section 4).

Our flow phantom results confirm that our custom-built gradient can allow substantial reductions in B_1 amplitude with no sacrifice in labeling efficiency. The curves in Fig. 3A depict the labeling efficiency (or the fraction of the equilibrium magnetization that remained aligned with B_{eff} at the end of the labeling process [2,20,21]) as a function of B_1 amplitude for five different gradient currents. As expected, each of the curves for the labeling efficiency, α, increased and reached a plateau as B_1 increased. The color-coded circles in the figure indicate $B_{1\,min}$, or the minimum amplitude of B_1 required to achieve 90% labeling

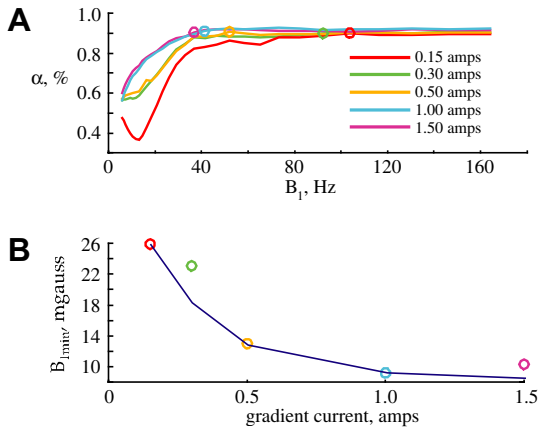

Fig. 3. (A) Shows flow phantom measurements of the labeling efficiency, α, as a function of B_1 amplitude with 5 different currents flowing through the custom-built gradient. As gradient current increased the curves for α shifted to the left, indicating that adiabatic conditions were being achieved with lower B_1 amplitude. The color-coded circles on each curve mark $B_{1\,min}$, or the minimum B_1 amplitude required for α to reach 90%. In (B) we have plotted these same $B_{1\,min}$ data points as a function of gradient current. We used our modeling tools to generate the solid line in this graph, which shows the predicted B_1 amplitude required to keep the maximum value of κ constant as the gradient current increased from 0.15 A. The excellent agreement between the predicted and flow phantom results validates the assumptions and algorithms we used to develop our model. Both the measured and predicted results clearly show that, when the gradient current is optimized, adiabatic conditions can be achieved with lower B_1 amplitude and hence lower SAR.

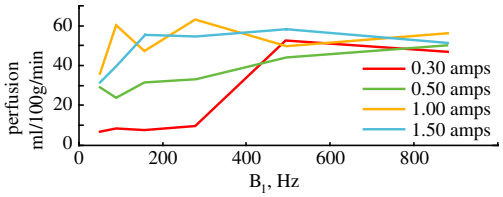

Fig. 4. These curves are similar to the flow phantom results shown in Fig. 3A but summarize in vivo results obtained from the rat hind limb. To increase the perfusion signal, all the measurements were acquired at least 4 min after initiation of stimulated exercise so that perfusion had reached a relatively high steady state. While the data here are noisier, the pattern is the same as that seen in Fig. 3; as gradient current increased the curves shifted to the left. For these particular conditions, $B_{1\,min}$ decreased from about 530 Hz to less than 210 Hz as the gradient current increased from 0.30 to 1.50 A.

efficiency. The key result in Fig. 3A is that, as the gradient current increased, the curves for α shifted to the left, indicating that the desired flow-driven, adiabatic excitation was occurring with lower B_1 amplitude. This is more easily seen in Fig. 3B, where we have plotted $B_{1\,min}$ as a function of gradient current. The pattern here is very clear; as the gradient current increased from 0.15 to 1.5 A, $B_{1\,min}$ decreased by a factor of 2.6 from 110 to 43 Hz.

Fig. 3B also includes modeling results (solid line) showing the predicted reduction in $B_{1\,min}$ allowed by optimizing the gradient current. To generate this curve we first used the model to calculate κ for the ΔB_0 field that we measured at 0.15 A (see Fig. 2A) with the B_1 field rescaled to a nominal amplitude of 110 Hz (i.e. to the measured value of $B_{1\,min}$ in the flow phantom measurements at 0.15 A). For these conditions, which correspond to the red dots in Fig. 3A and B, the model calculated that the nominal amplitude of the κ field would be 0.06. We then generated the remaining points on the curve by having the model calculate the B_1 amplitude that would yield this same nominal amplitude of κ for the ΔB_0 fields generated at each of the remaining gradient currents. In this way we used the model to predict $B_{1\,min}$ as a function of gradient current. We provide a more detailed explanation of the rationale behind these calculations in the Section 4. The excellent agreement between the predicted and measured changes in $B_{1\,min}$ validates the accuracy of our model.

We observed the same pattern in our in vivo measurements shown in Fig. 4. These single-voxel, gradient-enhanced FAWSETS perfusion measurements were acquired from exercising rat hind limb. For all gradient currents, the labeling efficiency, as reflected by the amplitude of the perfusion signal, increased and reached a plateau as B_1 increased. The data are noisier than those from our flow phantom experiments but the pattern is the same; as gradient current increased the curves shifted to the left. This verifies that flow-driven, adiabatic excitation of the arterial water was being achieved with lower B_1 amplitude as the gradient current increased. Under these particular conditions, $B_{1\,min}$ decreased from about 530 Hz to less than 210 Hz as the gradient current increased from 0.30 to 1.5 A. This represents a factor of 2.5 reduction in B_1 amplitude, which is almost identical to the reduction we observed in the flow phantom measurements in Fig 3.

We have also applied our modeling approach to predict the potential for shaped gradients to reduce SAR during the CASL labeling process. In Fig. 5 we present modeling results for three different cases; (1) using parameters for a typical CASL measurement [5,24], (2) using a uniform B_1 field of 170 Hz with an optimized ΔB_0 field and (3) using a uniform B_1 field of 64 Hz and the same optimized ΔB_0 field. The shapes of the ΔB_0 and B_{eff} fields (Fig. 5A and B) are considerably different for the shaped gradient than for the linear gradient but the evolution of ϕ (Fig. 5C) is nearly identical for both gradients. This demonstrates that the optimized ΔB_0 field can be designed so that it does not substantially increase the thickness of the region over which the adiabatic inversion takes place, which would increase relaxation losses during the labeling process (see Section 4). Another key point concerns the shapes of the κ fields in Fig. 5E. When the B_1 field with reduced amplitude is used with the optimized ΔB_0 field (dashed line) the shape of the κ field is very similar to the one corresponding to the typical CASL parameters (dotted line). As we explain further in the Section 4, this similarity allows the comparisons between the nominal amplitudes of the κ fields in order to predict the labeling efficiency. These results suggest that the optimized ΔB_0 field would allow B_1 to be reduced by a factor of 2.6, compared to the linear gradient, while keeping the nominal amplitude of κ

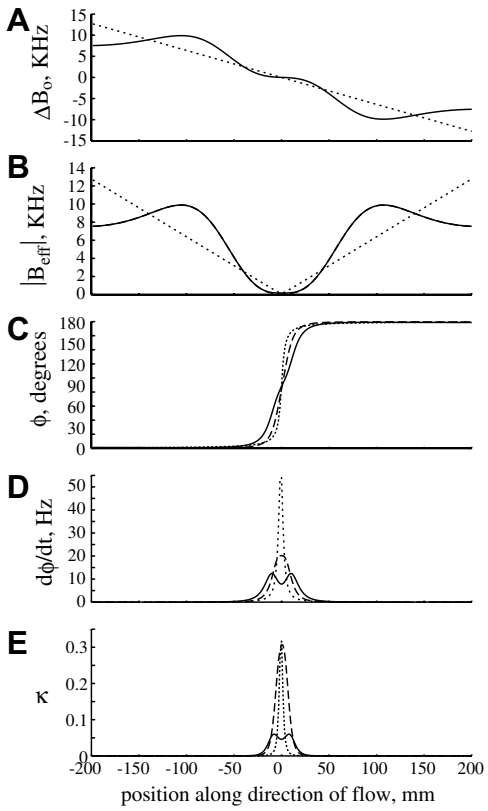

Fig. 5. These modeling results predict that optimizing the ΔB_0 field could also reduce SAR in CASL measurements. The parameters presented here are the same as those shown in Fig. 2. The dotted lines correspond to the conditions during a typical CASL labeling period; a uniform B_1 amplitude of 170 Hz and a linear B_0 gradient of 0.15 G/cm. The solid lines correspond to the same B_1 field but a ΔB_0 field shaped specifically for flow-driven adiabatic inversion. The dashed lines correspond to the shaped ΔB_0 field and a uniform B_1 field with the amplitude reduced to 65 Hz. (The solid line and the dashed line overlap in (A and B.) In (C) the dotted line and the dashed line nearly overlap, indicating that when a B_1 amplitude of 65 Hz is used in conjunction with the shaped ΔB_0 field, the thickness of the labeling slice is essentially the same as it is for a typical CASL measurement. (E) shows that, when B_1 is kept constant, the shaped gradient reduces the nominal amplitude of κ by a factor of 5 (from 0.31 to 0.06) when compared to the linear gradient. The dashed line in this figure shows that the shaped gradient allows B_1 to be reduced by a factor of 2.6 (from 170 to 65 Hz) while keeping the nominal amplitude and shape of the κ field approximately the same as it would be with a linear gradient. This would correspond to a factor of 6.76 reduction in SAR.

approximately the same. This corresponds to nearly a factor of 7 reduction in SAR.

4. Discussion

Flow-driven, adiabatic spin labeling is achieved by creating a spatially variant effective field that is initially aligned with the z-axis—and therefore parallel to the equilibrium magnetization of the flowing arterial water—and that smoothly evolves to the desired final orientation. If adiabatic conditions are maintained throughout the labeling process, the arterial water magnetization will remain aligned with B_{eff}. The final orientation of B_{eff} then determines the kind of labeling, inversion or excitation, the arterial spins undergo. The labeling efficiency, the fraction of the equilibrium magnetization that remains aligned with B_{eff} at the end of the labeling process, is determined by a number of factors including the amplitude of B_{eff}, the time rate of change of ϕ, the relevant relaxation rate during the labeling process ($T_{1\rho}$) and the time that the net magnetization vector has a significant component in the transverse plane as the spins flow through the labeling slice.

As shown by Garwood et al. [17,18], the most concise way to evaluate adiabatic manipulations is to use the adiabaticity ratio, κ, or the ratio of the angular velocity of B_{eff} to the precession frequency of the net magnetization vector, M, around B_{eff}. They have shown that the requirement for adiabatic RF pulses is that κ must remain much less than 1 at all times in order to maintain alignment between M and B_{eff}. They have also shown that the minimum B_1 amplitude required to keep κ much less than 1 is strongly dependent on the frequency sweep modulation function. These principles were developed for adiabatic RF pulses but they also apply to flow-driven adiabatic manipulations, where the ΔB_0 field is analogous to the frequency sweep modulation function, and they formed the basis of our modeling approach.

We used our model to evaluate the advantages of nonlinear ΔB_0 fields when applied to two different continuous ASL techniques: CASL, which results in inversion of flowing spins, and FAWSETS, which results in excitation of flowing spins. As described previously in greater detail [8,19] , the FAWSETS labeling process relies on gradients in both B_0 and B_1. The B_1 gradient occurs at the edges of the sweet spot of the RF coil where, by definition, the B_1 amplitude decreases. The shimming process creates the necessary B_0 gradient. Shimming creates a homogenous B_0 field within the B_1 sweet spot but leaves a gradient in B_0 at the edges of the sweet spot. These B_0 and B_1 gradients are sufficient, but not necessarily optimized, for generating flow-driven adiabatic excitation of flowing spins as they enter the sweet spot. While the ΔB_0 field generated by our custom-built gradient was not specifically designed to reduce the B_1 amplitude required to maintain adiabatic conditions, in our original publication on gradient-enhanced FAWSETS we speculated that it might allow some reductions [19]. In this work we provide modeling, flow phantom and in vivo results validating this claim.

4.1. Modeling of the FAWSETS labeling process

The modeling approach we implemented is described by the results shown in Fig. 2. The primary inputs to the model are B_1 and ΔB_0 described as functions of position along the direction of flow. For the FAWSETS modeling, we measured these fields (Fig. 2A) as generated by the RF coil and custom gradient that we previously developed for use in rat hind limb [19]. As expected the general shape of the ΔB_0 field remained constant but the amplitude increased in proportion to current flow in the gradient

circuit. After assuming a reasonable velocity of 10 cm/s we were able to make straightforward calculations of the remaining parameters depicted in Fig. 2. Note that, at all gradient currents, the peak value of $d\phi/dt$ occurred at or very near the plane where the magnitude of B_{eff} passed through a minimum. Hence κ, the ratio of $d\phi/dt$ to B_{eff}, always reached its maximum value in this plane. By increasing the gradient current we reduced the peak value of $d\phi/dt$, increased the minimum value of B_{eff} and shifted all the curves in Fig. 2 (except that for B_1, which was kept constant for all the calculations) to the right. All these changes worked in favor of reducing the maximum amplitude of κ.

The maximum gradient current we evaluated in Fig. 2, 1.5 A, was the highest current output available from the custom-built power supply we used to drive the gradient circuit. To explore the potential impact of higher gradient currents we scaled up the measured ΔB_0 field corresponding to 1.5 A and provided this hypothetical field as an input to the model in order to repeat the calculations of Fig. 2. The model predicted (data not shown) that the nominal amplitude of the κ field would continue to decrease for gradient currents higher than 1.5 A. But at gradient currents around 2.0 A the labeling slice, as measured by the regions where ϕ is evolving in Fig. 2B, began to encroach on the 8 mm thick sweet spot of the RF coil. This could lead to errors in the perfusion measurements. Hence, the optimal gradient current for this particular combination of gradient and RF coils seems to be about 1.8 A.

Both $d\phi/dt$ and κ are proportional to velocity, which we chose somewhat arbitrarily to be 10 cm/s. Selection of a different velocity would rescale the curves in Fig. 2D and E but the pattern of the results would be the same; as the flow of current in the gradient increased the nominal amplitude of κ would decrease. For in vivo applications, the expected velocity of the arterial spins depends on a number of factors, including the species and organ to be studied. Our modeling results show that, for a given velocity, the gradient current can be adjusted to reduce the amplitude of the κ field. It is reasonable to assume that optimizing the ΔB_0 in this way would allow adiabatic conditions to be achieved with lower B_1 amplitude and we conducted flow phantom measurements to test this assumption.

4.2. Validation by flow phantom measurements

Our flow phantom results confirm the accuracy of the model's predictions and demonstrate that, as the gradient current increased to 1.5 A, the ΔB_0 fields became more optimal for flow-driven adiabatic excitation, allowing progressive reductions in $B_{1\,min}$. In Fig. 3A the curves describing the labeling efficiency, α, as a function of B_1 amplitude consistently shifted to the left as the gradient current increased. This shows that α reached a plateau at lower B_1 amplitude as the gradient current increased. Under these particular conditions, as the gradient current increased from 0.15 to 1.5 A, $B_{1\,min}$ decreased by a factor of 2.6 (Fig. 3B), corresponding to a factor of 6.76 reduction in SAR, with no loss in labeling efficiency. We used the color-coded circles in these graphs to indicate $B_{1\,min}$, which we defined as the minimum nominal B_1 amplitude required to achieve 90% labeling efficiency. $B_{1\,min}$ is an important parameter because it defines the most efficient nominal B_1 amplitude for a given set of experimental conditions. For values of B_1 below $B_{1\,min}$, α decreases below its maximum value because adiabatic conditions are not maintained, at least not for faster flowing water. This would cause a decrease in the perfusion signal, reducing S/N and likely leading to artifacts when quantifying the signal. If B_1 is increased above $B_{1\,min}$ there is no substantial improvement in labeling efficiency so the amount of RF energy absorbed by the tissue would be improvidently high.

Hence, an important function for the model is the ability to predict $B_{1\,min}$ for a particular ΔB_0 field by rescaling the B_1 field as necessary to determine the minimum amplitude at which α reaches 90%. Our results in Fig. 2 demonstrate that the model can calculate κ for different combinations of ΔB_0 and B_1 fields. The next step was to use the calculated κ field to estimate α. There is no equation that allows direct calculation of α from κ so this step required us to make an assumption about the relationship between the two parameters. Our assumption is based on the observation that the curves for κ in Fig. 2E all have essentially the same shape, though they are shifted in position and differ in scale as a result of the different gradient currents. We found that this observation also holds true for a family of κ fields calculated by rescaling the measured B_1 field while holding the ΔB_0 field constant (data not shown). The position shifts do not affect α so we made the assumption that, for this particular case, the maximum amplitude of κ could be used to make reliable predictions of α. We note that, in general, the labeling efficiency depends not only on the maximum amplitude of κ but also on the pattern of its spatial variations so our assumption would not be valid when comparing κ fields with substantially different shapes.

We employed this assumption, along with the empirical results of Fig. 3A to test the ability of our model to predict $B_{1\,min}$ as a function of gradient current. To generate the first point in this curve, we provided the B_1 field and the ΔB_0 field measured at 0.15 A (both are shown in Fig. 2A) as inputs to the model but we rescaled the nominal amplitude of the B_1 field to 110 Hz. This rescaled B_1 field corresponds to $B_{1\,min}$ at 0.15 A, as shown in Fig. 3A. With these fields as inputs the model calculated the maximum amplitude of κ to be 0.06. That is, when the most efficient B_1 field, as determined empirically from the flow phantom measurements, was matched to this particular ΔB_0 field, the nominal amplitude of the resulting κ field was 0.06. Further increases in the amplitude of B_1 would decrease the amplitude of the κ field but, using our definition of $B_{1\,min}$ given above, this would increase tissue heating with no further increase in labeling efficiency. These results established the optimal amplitude of the κ field and we were then able to use our model to predict the nominal

B_1 amplitude that would yield the same maximum amplitude of κ for each of the other four measured ΔB_0 fields. The results of these calculations form the remaining points along the solid line in Fig. 3B. The excellent agreement between these predicted values of $B_{1\,min}$ and the measured values, taken from Fig. 3A, validate our modeling approach and the assumptions we made concerning the relationship between κ and α. Further, these results demonstrate that the model can be used to predict $B_{1\,min}$ for other combinations of ΔB_0 and B_1 provided that the shapes of the κ fields being compared are similar.

4.3. Validation by in vivo measurements

Our rat hind limb measurements (Fig. 4) provide further confirmation of the validity of our modeling approach and demonstrate a practical application where nonlinear gradients can be used to reduce SAR. For these in vivo measurements we did not directly measure the labeling efficiency but the shapes of the curves describing the perfusion signal are very similar to those for α in Fig. 3A and reflect the expected relationship between labeling efficiency and B_1 amplitude. For all gradient currents shown in Fig. 4 the curves for the perfusion signal gradually increased and reached a plateau as the B_1 amplitude increased. The plateau occurred at about 50 ml/100 g/min, which is in agreement with our previous FAWSETS measurements in exercising rat hind limb muscle [10]. As with the flow phantom data, the curves for the perfusion signal consistently shifted to the left as the gradient current increased, indicating that the labeling efficiency reached its maximum value at lower B_1 amplitude. In these measurements optimizing the gradient current allowed us to reduce B_1 by a factor of 2.5, providing essentially the same improvement predicted by our model and measured in our flow phantom experiments.

4.4. Modeling of the CASL labeling process

We also present modeling results showing that substantial reductions in B_1 amplitude could be achieved by implementing custom gradients in CASL measurements (Fig. 5). In CASL measurements, the ΔB_0 field is typically generated by the linear gradients provided as standard equipment in modern MR imaging systems. While they are not optimized for effective labeling, these linear gradients are used for convenience and to avoid the expense of building separate gradient inserts dedicated to CASL measurements.

Frank et al. [14] and Richardson et al. [25] have demonstrated the utility of custom-built gradients in CASL measurements of human leg perfusion. Their custom-built gradient volume coil, integrated with their birdcage style RF coil, was designed primarily to overcome the performance limitations of their built-in gradient coils. Trampel et al. [12] used a combination of gradient and RF surface coils to implement two-coil CASL measurements of human brain perfusion. In both these applications, the custom-built gradients were deliberately designed to generate a magnetic field that varied linearly with position along the direction of arterial flow.

Our modeling results (Fig. 5) predict that a nonlinear ΔB_0 field could substantially reduce the potential for tissue heating during CASL labeling. The modeling approach we implemented here was the same as for Fig. 2 except that we could not measure ΔB_0 since we have not yet built a gradient for CASL measurements. Instead, we used an iterative approach to design an appropriate ΔB_0 field.

The curves for ϕ in Fig 5C highlight an important constraint that must be considered when optimizing the ΔB_0 field. It is relatively easy to reduce the B_1 amplitude and still maintain adiabatic conditions if the thickness of the labeling slice is allowed to increase substantially. This can be achieved simply by reducing the amplitude of a linear gradient. The problem with this approach is that it would increase $T_{1\rho}$ relaxation losses because it would take longer for the arterial water to flow through the labeling slice. The curves describing ϕ in Fig. 5C demonstrate that the ΔB_0 field can be optimized without significantly increasing the thickness of the labeling slice.

The κ field corresponding to the optimized ΔB_0 field and the reduced amplitude B_1 field (dashed line in Fig 5E) is similar in both shape and amplitude to the κ field corresponding to the typical CASL parameters (dotted line). Using the same reasoning we applied to interpret the flow phantom measurements above, this similarity suggests that the labeling efficiency would be about the same in both cases. Hence, the model predicts that an optimized ΔB_0 field could allow the B_1 amplitude to be reduced to 64 Hz in an application that would require 170 Hz if a linear gradient were used. This factor of 2.6 reduction in B_1 corresponds to a factor of 6.76 reduction in SAR, a substantial improvement that may well justify the cost and complexity of a custom gradient insert.

5. Conclusions

We have implemented a model of the flow-driven, adiabatic spin labeling process that calculates the spatial variations in κ for different combinations of ΔB_0 and B_1 fields. The model predicted that custom-built magnetic field gradients could allow reductions in the B_1 amplitude and thereby reduce SAR during the FAWSETS labeling process by a factor of about 6.25. Our flow phantom and in vivo measurements verified the model's predictions and the assumptions we used to interpret them. Our model also predicted that similar reductions in SAR could be achieved by employing custom-built gradients in CASL measurements.

This work focused specifically on the B_1 and ΔB_0 fields generated by our RF and gradient coils that we built for use in rat hind limb. While the strong agreement between our modeling predictions and our flow phantom and in vivo results demonstrates that the basic physical principles we employed are sound, the generality of our approach

remains to be determined. The actual reductions in SAR that can be achieved with a nonlinear gradient designed for human applications will likely vary, depending on the organ to be studied and other experimental conditions. In the particular animal protocol we have explored here the SAR without gradient enhancement was about 1 W/kg (see Section 2) and the additional cost required to build and implement a custom gradient insert would not be necessary. However, tissue heating is clearly a concern in many ASL measurements, particularly at higher magnetic fields, and the approach we have described here could make the critical difference between safe and unsafe measurements in some experiments.

Acknowledgments

This study was supported by National Institutes of Health Grant HL64946 and a grant from the University of Washington's Royalty Research Fund.

References

[1] G. Zaharchuk, P.J. Ledden, K.K. Kwong, T.G. Reese, B.R. Rosen, L.L. Wald, Multislice perfusion and perfusion territory imaging in humans with separate label and image coils, Magn. Reson. Med. 41 (1999) 1093–1098.
[2] H.M. Gach, A.W. Kam, E.D. Reid, S.L. Talagala, Quantitative analysis of adiabatic fast passage for steady laminar and turbulent flows, Magn. Reson. Med. 47 (2002) 709–719.
[3] D.G. Norris, High field human imaging, J. Magn. Reson. Imaging 18 (2003) 519–529.
[4] M.A. Fernandez-Seara, Z. Wang, J. Wang, H.Y. Rao, M. Guenther, D.A. Feinberg, J.A. Detre, Continuous arterial spin labeling perfusion measurements using single shot 3D GRASE at 3T, Magn. Reson. Med. 54 (2005) 1241–1247.
[5] Z. Wang, J. Wang, T.J. Connick, G.S. Wetmore, J.A. Detre, Continuous ASL (CASL) perfusion MRI with an array coil and parallel imaging at 3T, Magn. Reson. Med. 54 (2005) 732–737.
[6] T. Mildner, R. Trampel, H.E. Moller, A. Schafer, C.J. Wiggins, D.G. Norris, Functional perfusion imaging using continuous arterial spin labeling with separate labeling and imaging coils at 3T, Magn. Reson. Med. 49 (2003) 791–795.
[7] S.L. Talagala, F.Q. Ye, P.J. Ledden, S. Chesnick, Whole-brain 3D perfusion MRI at 3.0 T using CASL with a separate labeling coil, Magn. Reson. Med. 52 (2004) 131–140.
[8] K. Marro, FAWSETS: flow-driven arterial water stimulation with elimination of tissue signal, J. Magn. Reson. 124 (1997) 240–244.
[9] K.I. Marro, O.M. Hyyti, M.A. Vincent, M.J. Kushmerick, Validation and advantages of FAWSETS perfusion measurements in skeletal muscle, NMR Biomed. 18 (2005) 226–234.
[10] K.I. Marro, O.M. Hyyti, M.J. Kushmerick, FAWSETS perfusion measurements in exercising skeletal muscle, NMR Biomed. 18 (2005) 322–330.
[11] E.C. Wong, A. Jesmanowicz, J.S. Hyde, Coil optimization for MRI by conjugate gradient descent, Magn. Reson. Med. 21 (1991) 39–48.
[12] R. Trampel, T. Mildner, U. Goerke, A. Schaefer, W. Driesel, D.G. Norris, Continuous arterial spin labeling using a local magnetic field gradient coil, Magn. Reson. Med. 48 (2002) 543–546.
[13] L.R. Frank, E.C. Wong, W.M. Luh, J.M. Ahn, D. Resnick, Articular cartilage in the knee: mapping of the physiologic parameters at MR imaging with a local gradient coil–preliminary results, Radiology 210 (1999) 241–246.
[14] L.R. Frank, E.C. Wong, L.J. Haseler, R.B. Buxton, Dynamic imaging of perfusion in human skeletal muscle during exercise with arterial spin labeling, Magn. Reson. Med. 42 (1999) 258–267.
[15] R.S. Richardson, E.A. Noyszewski, L.J. Haseler, S. Bluml, L.R. Frank, Evolving techniques for the investigation of muscle bioenergetics and oxygenation, Biochem. Soc. Trans. 30 (2002) 232–237.
[16] A. Tannus, M. Garwood, Adiabatic pulses, NMR Biomed. 10 (1997) 423–434.
[17] M. Garwood, L. DelaBarre, The return of the frequency sweep: designing adiabatic pulses for contemporary NMR, J. Magn. Reson. 153 (2001) 155–177.
[18] M. Garwood, K. Ugurbil, B1 Insensitive Adiabatic RF Pulses NMR Basic Principles and Progress, Springer, New York, 1992, pp. 109-147.
[19] K. Marro, D.H. Lee, O.M. Hyyti, Gradient-enhanced FAWSETS perfusion measurements, J. Magn. Reson. 175 (2005) 185–192.
[20] K.I. Marro, C.E. Hayes, M.J. Kushmerick, A model of the inversion process in an arterial inversion experiment, NMR Biomed. 10 (1997) 324–332.
[21] L. Maccotta, J.A. Detre, D.C. Alsop, The efficiency of adiabatic inversion for perfusion imaging by arterial spin labeling, NMR Biomed. 10 (1997) 216–221.
[22] F.Q. Ye, V.S. Mattay, P. Jezzard, J.A. Frank, D.R. Weinberger, A.C. McLaughlin, Correction for vascular artifacts in cerebral blood flow values measured by using arterial spin tagging techniques, Magn. Reson. Med. 37 (1997) 226–235.
[23] A.J. Schwarz, M. Rijpkema, D.J. Collins, G.S. Payne, T. Prock, A.C. Woodward, A. Heerschap, M.O. Leach, SAR and tissue heating with a clinical (31)P MRS protocol using surface coils, adiabatic pulses, and proton-decoupling, Magn. Reson. Med. 44 (2000) 692–700.
[24] W. Zhang, D.S. Williams, J.A. Detre, A.P. Koretsky, Measurement of brain perfusion by volume-localized NMR spectroscopy using inversion of arterial water spins: accounting for transit time and cross-relaxation, Magn. Reson. Med. 25 (1992) 362–371.
[25] R.S. Richardson, L.J. Haseler, A.T. Nygren, S. Bluml, L.R. Frank, Local perfusion and metabolic demand during exercise: a noninvasive MRI method of assessment, J. Appl. Physiol. 91 (2001) 1845–1853.